# Hard x-rays, ejecta, and their associated decimetric radio emission in solar flares

Pascal Saint-Hilaire[1,2] and Arnold O. Benz[1]
[1] *Institute of Astronomy, ETH Zentrum, CH-8092 Zurich, Switzerland* (`shilaire@astro.phys.ethz.ch`)
[2] *Paul Scherrer Institute, CH-5232 Villigen, Switzerland*

**Abstract.** We investigate temporal and spatial correlations in solar flares of hard X-rays (HXR) and decimetric continuum emissions, ejecta, and CMEs. The focus is on three M class flares, supported by observations from other flares. The main conclusions of our observations are that (1) major hard X-ray flares are often associated with ejecta seen in soft X-rays or EUV. (2) Those ejecta seem to start before HXR or related decimetric radio continua (DCIM emission). (3) DCIM occuring nearly simultaneously with the first HXR peak are located very close to the HXR source. Later in the flare, DCIM generally becomes stronger, drifts to lower frequency and occurs far from the HXR source. Thus the positions at high frequency are generally closer to the HXR source. DCIM emission consists of pulses that drift in frequency. The very high and sometimes positive drift rate suggests spatially extended sources or type III like beams in an inhomogenous source. Movies of selected flares used in this study can be found on the CD-ROM[1] accompanying this volume.

**Keywords:**

[1] http://www.astro.phys.ethz.ch/papers/shilaire/HXRDCIM_CDROM_material/

## 1. Introduction

The release of non-potential magnetic energy in the corona accelerates charged particles to supra-thermal energies. Accelerated particles emit a variety of temporary radiations generally termed *flares*. Depending on wavelength and type of emission, they yield information on the propagation, thermalization and further development of the flare energy. Most prominent are hard X-rays (HXR, $\gtrsim$10 keV) emitted as bremsstrahlung of energetic electrons losing energy by collisional interactions. They yield estimates of flares energies with a range beyond $10^{32}$erg, of the number of accelerated electrons up to $10^{38}$, and of electron energies up to 100 MeV. Other emissions include gyrosynchrotron radiation from decimeter to millimeter waves, produced by relativistic electrons in kilogauss magnetic fields, and gamma-ray lines due to impinging energetic ions.

The common feature of all the above emissions is that they are produced by energetic particles, the product of acceleration. The region of emission is usually not the acceleration site, but some target plasma often at higher density and lower altitude. Thus the emissions give only indirect information on the acceleration process that has remained enigmatic for this reason since many decades. The theoretical work has recently concentrated on stochastic acceleration by Transit-Time Damping, but field aligned electric fields and shock waves may also play a role (cf. review by Miller et al., 1997).

It is surprising that the very process of acceleration of such overwhelming dimensions in our astronomical neighborhood should be hidden to direct observation. It is not even clear where acceleration occurs. The large number of electrons and the huge amount of energy involved point to a low altitude for the energy release site. On the other hand, time-of-flight measurements of electrons at different energies using HXR peaks rather suggest a high injection site (Aschwanden et al. 1998).

Coherent radio emissions, characterized by relatively small bandwidths and high polarization, have been observed during flares from meter wavelengths up to 8 GHz (Bruggmann et al. 1990). Such emissions are sensitive signatures of deviations from thermal electron distributions driving plasma instabilities. In particular, beams of electrons, trapped electrons, unstable currents and shocks are known or suspected sources of coherent radio emission. They are radiated at the local plasma frequency, upper hybrid frequency, electron gyrofrequency, or their low order harmonics. Therefore, the observed range of coherent bursts includes source densities up to $4\times10^{11}$cm$^{-3}$ (second harmonic) and magnetic field strengths up to about 1000 G (third harmonic).

These limits include the plasma parameters generally expected in the flare acceleration site (e.g. Miller at al., 1998). Thus, the decimeter wavelengths are the range to search for coherent emissions from the accelerator.

Extremely narrowband and short spikes at decimeter waves (reported in the range 200 MHz to 8 GHz) have been suspected to be more directly related to the acceleration site than any other emission. The hypothesis includes two parts: spatial coincidence of the radio source and the acceleration site as well as a similarly high degree of fragmentation (Benz, 1986). Evidence comes mainly from the excellent correlation of spikes at meter waves and type III radio bursts, which sometimes seem to emanate from a group of metric spikes in the spectrum (Benz et al., 1996) and in space (Paesold et al., 2001). However, these metric spikes and type III bursts are often not associated with reported HXR emission and tend to have no counterparts in H$\alpha$. Furthermore, their location is high in the corona, and the energies involved are small (less than $10^{27}$ erg, Krucker et al., 1995). On the other hand, spikes in the *decimeter range* are well associated with HXR emission. However, the converse is not true: HXR bursts are associated with decimetric spikes only to $\geq$2% (Güdel et al., 1991). Decimetric spikes are thus at most a sporadic signature of acceleration. This is also the conclusion of a recent investigation of the temporal and spatial association of decimetric spikes with HXR and thermal flare emissions (Benz et al., 2002).

Various forms of "pulsations" or broadband fluctuations have been known to occur in the decimeter range before, during, and after flares (cf. catalogues by Güdel and Benz, 1990; Isliker and Benz, 1994). A very regular subtype of them has been interpreted as MHD oscillation of a magnetic flux tube containing trapped electrons and modulating their emission due to a loss-cone velocity distribution (Roberts and Mangeney, 1982) or as a limit cycle (Lotka-Volterra type) oscillation between precipitation and loss-cone instability (Aschwanden and Benz, 1988). Only 20% of those regular pulsations are associated with HXR emission, in which case the correlation is generally weak (Aschwanden et al., 1990). More recently, Kliem et al. (2000) have studied an event of irregular pulsations associated with HXR emission. The radio burst consists of irregular pulses with a bandwidth of 500 MHz at a center frequency of initially 1.5 GHz, drifting to lower frequency in the course of the event. The authors interpret the radio emission as a direct signature of reconnection. Similar events have been studied by Hori (1999), Khan et al. (2002), Karlicky et al. (2002), and others.

The previous studies have selected a certain type of radio burst and searched for associated HXR. Here we present a study applying the opposite approach: major HXR events have been selected and their radio emission in decimeter waves are studied in the spectrum and location relative to the HXR source. The HXR source is taken as indication for the site of prime flare energy deposition. A first step is to find direct radio signatures of the acceleration process, as close in time and space as possible. If such an emission exists, the radio spectrum can be used to investigate the nature of the emission and possibly reveal properties of the acceleration process.

## 2. Instruments and data selection

Our investigation combines temporal and spatial data on HXR emission with spectral and spatial information on associated radio emission at decimeter wavelengths. In addition, SXT and EUV images of the thermal coronal plasma background were used to put the non-thermal sources into the general context of the associated active region.

### 2.1. The YOHKOH Hard X-ray Telescope (HXT)

HXT (Kosugi et al., 1991) imagery has a spatial resolution of 5 ". It sees mostly the HXR produced by the bremsstrahlung of non-thermal electrons hitting the chromosphere or lower corona. Those high energy electrons are presumably accelerated by the flare process occuring in the corona, and are hurled along magnetic field lines into the denser chromosphere. The HXT has four energy channels. In this investigation, only the lowest channel (14-23 keV) was used for imaging, as it usually has the most counts.

### 2.2. The Phoenix-2 spectrometer

The Phoenix-2 (Messmer et al., 1999) radio spectrometer was programmed to observe the low decimeter range simultaneoulsy with the Nançay Radioheliograph several months per year. The resulting spectrograms have a time resolution of 0.1 seconds, a frequency resolution of 1 MHz, and span the 220-553 MHz range. The Sun is surveyed continually (from sunrise to sunset). Stokes I and V data are usually available, except for part of 1999, where only one (linear) polarization was measured. The spectrograms have been background-subtracted, and some channels with interferences were removed.

### 2.3. The Nançay Radioheliograph (NRH)

The NRH (Kerdraon & Delouis, 1996) surveys and images the Sun continually at the following frequencies: 164, 236.6, 327, 410.5 and 432 MHz. Used NRH data were of two types:

- 120 ms time resolution, with 30" pixel resolution
- 10 seconds integrated data, with 15" pixel resolution

The second set[1] was used most often, as it has higher pixel resolution, takes less space on the hard disk, and the low time resolution is good enough for our needs.

The instrument has a nominal half-beamwidth of 1.96 arcmin at 164 MHz. It gets proportionally better at the higher frequencies. The relative accuracy (in arcseconds) of the position of a source centroid is hence given by the formula $\frac{118"}{\sigma}\frac{164}{\nu}$, where $\sigma$ is the signal-to-noise ratio, and $\nu$ the frequency in MHz. The absolute accuracy of NRH maps is of the order of 50".

### 2.4. The Yohkoh Soft X-ray Telescope (SXT)

The SXT (Tsuneta et al., 1991) provides full and partial disk images in the 0.25-4 keV range (i.e. sensitive to plasmas $\geq$ 2 MK), with pixel sizes down to 2.45". It monitors mostly the bremsstrahlung emission of the thermal plasma present in the corona. Five different filters can be positioned in front of the detector array to estimate isothermal temperatures and emission measures.

### 2.5. The Transitional and Coronal Explorer (TRACE)

TRACE (Handy et al., 1999) observations were carried out mostly with filters having the following wavelength bands:

- 1600Å : (bandwidth of 275Å, temperature range: 4.0-10.0 kK) sees chromospheric material in quiescence: the UV continuum, the CI and FeII lines, as well as the 200 kK CIV line in flares.
- 171Å: (bandwidth of 6.4Å, temperature range: 0.16-2.0 MK) sees coronal material: the FeIX and FeX lines.

As TRACE images tend to have an offset (of up to about 10 ") in their pointing, they have been shifted in order to fit more properly the Sun's limb (or EUV limb, for the EUV images), as best as was visually possible.

[1] http://mesola.obspm.fr/

### 2.6. Other data

We have supplemented the set of data if necessary by observations from the Ondrejov spectrograph (0.8 to 4.5 GHz) (Jiricka et al., 1993) and the CGRO-BATSE (Fishman et al., 1989) instrument, which can detect photons in the 25 to 1000 keV range.

### 2.7. Selection of Events

The events have been selected according to the following criteria:

- Intensive HXR emission: as a proxy for HXR, we used the NOAA (National Oceanographic and Atmospheric Administration) Solar Event Report [2], looking for gyrosynchroton radio emission above 10 GHz.

- Yohkoh HXT imagery had to be available, in order to determine the HXR sources' positions.

- Simultaneous Phoenix-2 spectrograms were required, showing decimetric radio continua (DCIM). The frequency range for those spectrograms must be 220-550 MHz in order to include the frequencies observed by the NRH.

- For position information of the bursts seen by Phoenix-2, radio imaging data from the NRH were mandatory.

- The events had to be as close to the limb as possible, where spatial information usually becomes more straightforward to use, and projection effects are less severe. This condition practically translated into taking events with locations beyond 45 degrees of solar longitude (east or west), as given by the NOAA Solar Event Report.

- To observe the spatial structure and temporal evolution of coronal loops, either Yohkoh SXT or TRACE images during each event were also required.

Very few events between 1999 and mid-2001 fulfilled all these stringent criteria, and had data deemed good enough for our study. A total of nine events were investigated. Three events (Table I) had data that could be considered as 'nearly ideal' in all respects: all instruments in sunlight, looking at the same region of the Sun, and getting useful data. They will be the ones used in this study, although several other events,

[2] gopher://sec.noaa.gov/11/indices

with poorer and/or partial data, were also examined closely to support the observations and conclusions made from the three best events.

On the CD-ROM accompanying this paper, movies (in mpeg or javascript format) can be found of the three main events, and also of numerous other events. All movies show TRACE or SXT images, with overlaid contours from the NRH and HXT. See the *index.html* page on the CD-ROM for further details. Most of the images shown in this paper are actually snapshots from these movies, to illustrate the points that we want to emphasize. No doubt that the movies themselves provide an almost endless amount of additional details, but they are beyond the scope of this paper. Here, we concentrate on a few major results.

## 3. Observations and results

Table I summarizes some characteristics pertaining to each of our three main events. Although they were not selected for these properties, all three had an ejecta observable in EUV or SXR, and meter wave type III bursts. Table II, shows that most selected flares seem to have some kind of an ejecta, while metric type III bursts are not always witnessed.

### 3.1. HXR/SXR/EUV observations

All three main events displayed an ejection of matter. It is clear from Figs. 1 and 4 that the observed ejection of matter occured before any HXR emission. The movie accompanying this volume shows an ejecta lifting at about 12:10 UT, three minutes before the start of any HXR emission, for the 1999/09/08 event. For the 2000/08/25 event, the first available SXT image (14:27:42 UT) already shows an ejecta $\sim$40" above the HXR-emitting region (the image of Fig. 2a was taken slightly later, but is of better quality). The ejecta velocity was estimated from successive SXT images to be $\sim$300 km/s (Table I), placing the start of the ejecta (assuming it originated in the HXR-emitting region) at $\sim$14:26 UT, just at the beginning of enhanced HXR flux, 1.5 minutes before peak HXR flux (Fig. 5). For the 2001/06/15 event, the ejecta was observed to be flung before 10:05 UT, again at the beginning of HXR emission (Figs 3 and 6), and $\sim$2 minutes before the peak of the HXR flux. As a proxy for HXR emission during early phases of HXR emission for the 2001/06/15 event, the time-derivative of GOES-8 SXR lightcurves were used. HXT lightcurves (and images) are available starting at 10:20 UT.

As seen in the HXR time profiles (Figs. 4, 5, & 6), there are several HXR peaks in each event. Ejection of material seem to occur only before

Table I. Observations summary for three prime events

| Event | 1999/09/08 | 2000/08/25 | 2001/06/15 |
|---|---|---|---|
| Class | M1.4 | M1.4 | M6.3 |
| AR | 8690 | 9143 | 9502 |
| Ejecta start time | 12:08 to 12:12 | ? | 10:02 to 10:05 |
| HXR peak time(s) | 12:14:00,12:14:40, 12:14:30 | 14:27:35, 14:31:00, 14:32:20 | $\sim$10:07:20, 10:27:00, 10:30:30, 10:49:00 |
| radio peak flux time 1.4 GHz | 12:15 | 14:28:02, 14:31:47 | $\sim$10:10, 10:27, 10:48:50 |
| peak flux time 327 MHz | 12:20:37 | $\approx$14:24(small), 14:31:39 | 10:07:22(typeII),$\approx$10:14, 10:34:29,10:49:00,11:02:23 |
| Brightness Temperature of brightest NRH pixel at peak flux (327 MHz) | 150 MK | $>$ 6000 MK | 100 MK |
| pulse duration pulsation period | 0.5 secs 4-30 secs | 0.4 secs $\approx$8 secs | $\approx$ 0.4 secs 2.4 secs |
| Overall Drift rate (MHz/s) | -1.56 at 328 MHz (950 km/s) | -2.8 at 420 MHz (1200 km/s) | -4.3 MHz/s at 412 MHz |
| Drift rate of pulses (MHz/s) | $>$ 1000 MHz/s at 430MHz | $>$ 1300 MHz/s at 477MHz | -1190 MHz/s at 535 MHz |
| proj. radio source motion DCIM, 327 MHz | 150 km/s | $>$300km/s | 450 km/s |
| projected ejecta speed (km/s) | 100 - 400 km/s | $\approx$300 km/s | 480 km/s |
| associated metric type III ? | starting right at 1st HXR peak | starting $\sim$2 min. after first HXR peak | starting $\sim$50s after HXR peak Type II starting $\sim$30s after HXR peak |
| associated decimetric type III ? | none observed | (faint) starting to occur $\sim$4 min. before HXR peak | (faint) starting to occur $\sim$50s before HXR peak |
| HXR footpoint separation (Mm) | 15" | 17" | (35"), (HXR spikes all over), (35", same FPs as before) |
| distance nearest radio source to HXR (peak HXR flux) | 10" (432MHz) | 80" | 20" other peaks: 90",90" |
| distance nearest radio source to HXR (peak radio flux) | 90" (327 to 432 MHz) | 100" | 85" (SW) (100" (S) at 10:49) |

Table II. Some additional characteristics pertaining to the examined flares. A '?' symbol means the data was not good enough for a clear-cut determination.

| Day | Time (UT) | Presence of meter type IIIs ? | EUV/SXT ejecta ? | Presence of CME ? |
|---|---|---|---|---|
| 1999/09/08 | 12:15 | yes | yes | no (?) |
| 2000/08/25 | 14:28 | yes | yes | yes |
| 2001/06/15 | 10:07 | yes | yes | yes |
| 1999/06/11 | 11:16 | no | ? | yes |
| 1999/06/12 | 13:31 | no | ? | no |
| 2000/07/07 | | no | ? | yes |
| 2000/07/12 | 10:31 | yes | ? | yes |
| 2000/08/12 | 09:50 | yes | yes | yes |
| 2000/09/14 | 14:40 | yes | yes | no |

or at the beginning of the first HXR peak in all three cases, and no ejecta was witnessed associated with subsequent HXR peaks.

HXR emission seen in our events generally has the double footpoint shape (see Figures 1c, 2a, and 3a). Some events (1999/09/08, 2001/06/15) showed HXR emission of different peaks to occur at the same places, while others (2000/08/25, 2001/06/15) showed slightly displaced (a few ") source locations (but with one of the footpoints remaining at the same place during all HXR flux peaks). The apparent HXR source sizes seem to be always close to about 5". Since this corresponds to HXT's spatial resolution, it indicates that the sources are not resolved.

For the 1999/09/08 event, comparing SXT difference images and the EUV ejecta (Fig. 7a), it is seen that the SXT increasing part (positive in the difference image) leads the EUV ejecta front by 5 to 10 arcseconds, whereas the SXT decreasing part (negative in the difference image) superposes well on the EUV ejecta. The isothermal temperature (using the ratio of SXT's AlMg and Al12 filters) and density in different parts of the AR at HXR peak time are shown in Table III. The SXT ejecta is remarkably hot and dense whereas the following cavity is even hotter, but an order of magnitude less dense. Apparently coincident with the ejecta is a much cooler plasma emitting C IV (observable with TRACE 1600 Å).

SXR emission measure $EM$ is $\int n^2 A\, dl$, where $A$ is the pixel area (in $cm^2$) and we integrate over the line-of-sight length of the column of material. This path length was approximated to be equal to the smallest dimension for features with a clearly dominant dimension (transverse to the line-of-sight) such as a thin loop, or the square root of the feature's

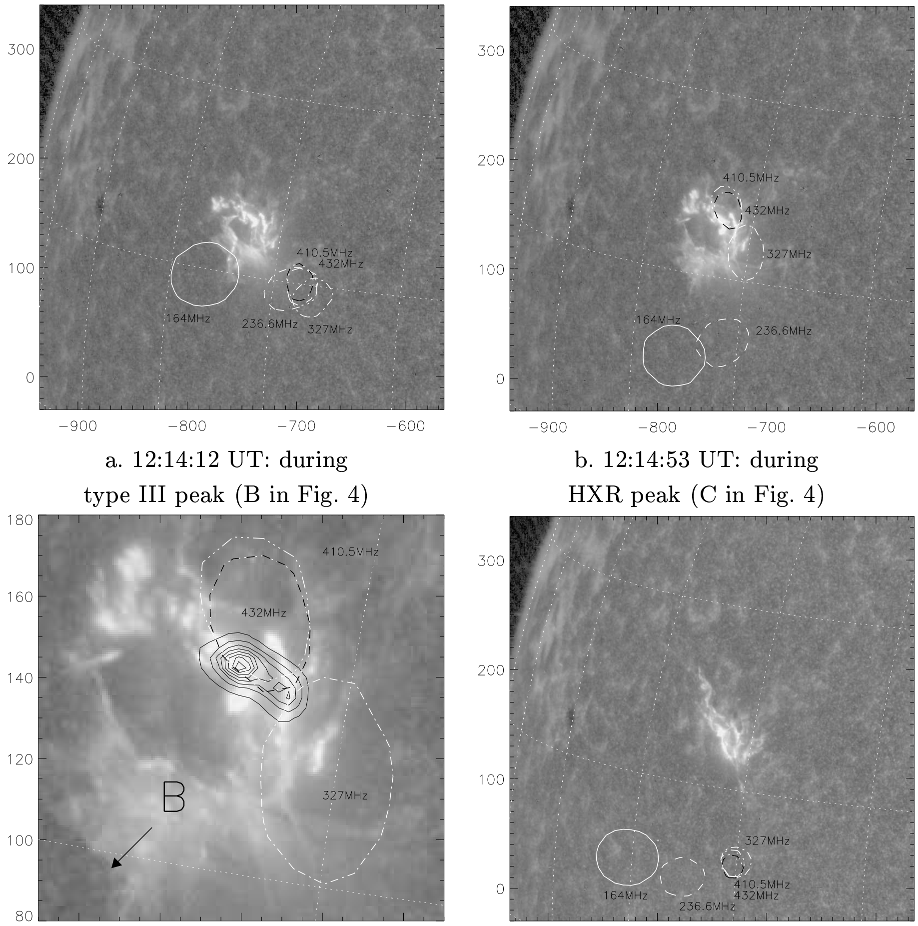


a. 12:14:12 UT: during type III peak (B in Fig. 4)

b. 12:14:53 UT: during HXR peak (C in Fig. 4)

c. 12:14:53 UT: during HXR peak (zoomed)

d. 12:20:08 UT: during DCIM peak phase (E in Fig. 4)

*Figure 1.* 1999/09/08 double-ribbon flare: TRACE 1600Å images with NRH contours (98% level) at various frequencies, and HXT (23-33 keV band) overlay (solid isophotes in c). The units of the axes are arcseconds from Sun center. The ejecta ('B') and its motion (arrow) are marked in c.

area if both length and width were of the same order. The electron density $n$ is assumed constant along the integration path.

Table III reveals that, of the SXR emitting region, only the cavity ('A' in Table III) between the ejecta and the AR is of low enough density to allow for radio emission as seen by NRH. NRH sees radio emission to the right of this cavity (Fig. 1 b and c).

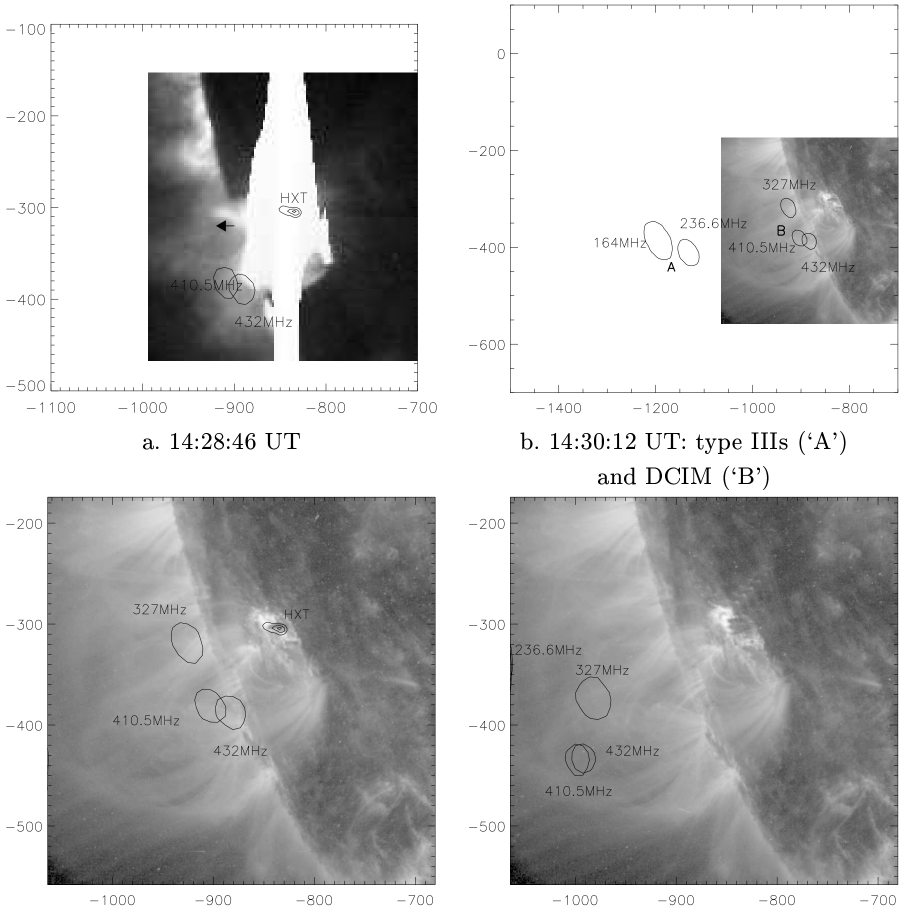


a. 14:28:46 UT

b. 14:30:12 UT: type IIIs ('A') and DCIM ('B')

c. 14:30:12 UT: zoomed

d. 14:33:48 UT: end of DCIM phase

*Figure 2.* 2000/08/25 Event. SXT AlMg and TRACE images with NRH and HXT (from 14:27:30) overlays. The SXT AlMg image (with some saturated pixels) shows an ejected plasmoid (arrow).

## 3.2. Radio observations

As can be seen from all radio spectrograms (Fig. 4, 5, and 6), metric type III radio bursts occurred shortly (almost immediately for the 1999/09/08 event, after ∼2 min for the 2000/08/25 event) after the first HXR peak in all of our three main events. Event 2001/06/15 even had a type II burst, indicating a shock wave. In all cases those type III bursts occured high above the AR, in the general direction where the main ejecta will later be headed. (Figs. 1a, 2a, 3a). The 2000/08/25 event also had a group of type IIIs occuring during the subsequent HXR peaks.

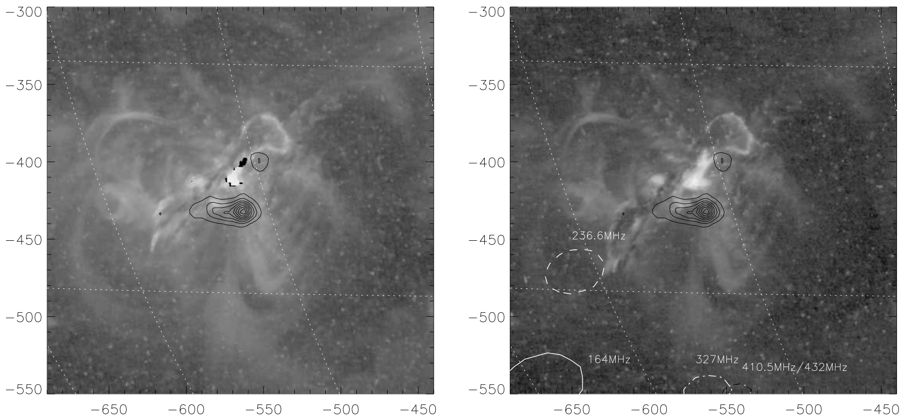


a. 10:06:54 UT: first HXR phase

b. 10:07:21 UT: type II phase ('A' in Fig. 6)

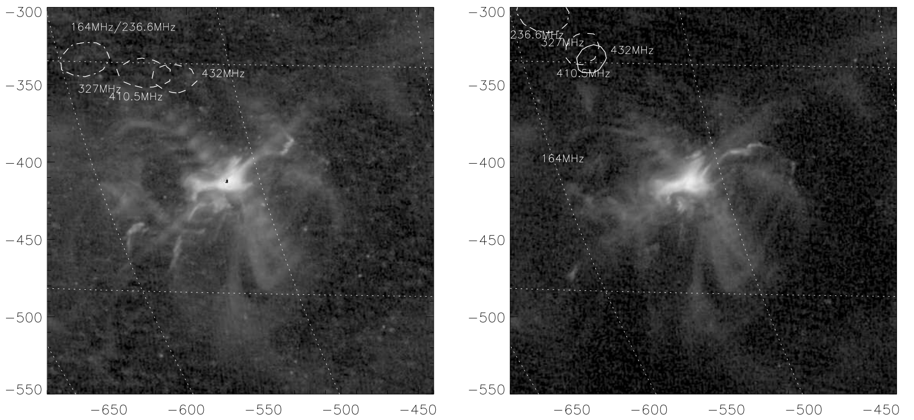


c. 10:09:23 UT: DCIM phase (start) ('C' in Fig. 6) and type IIIs ('B' in Fig. 6)

d. 10:12:24 UT: DCIM phase (peak time) ('C' in Fig. 6)

*Figure 3.* 2001/06/15 event: TRACE images with NRH (98% level) contours at various frequencies, and HXT (10:21 UT) overlay.

Still in the low frequency range, a few minutes afterwards, there are decimetric pulsations, coming sometimes in patches of varying intensities. These decimetric pulsations (dubbed 'decimetric pulsating structures', or DPS by Khan et al., 2002), actually start with the first HXR peak, as clearly demonstrated by high frequency spectrograms (1 GHz and more), and drift to lower frequencies. The drift rate in the low frequency (220-550 MHz) range is about minus 2 or 3 MHz/s (see Table I). Individual pulses have a 0.5 to 1 second duration, and occur at intervals of 4 to 30 seconds. In the 1999/09/08 and 2001/06/15 events, these DPS seem to stay in the loop structures near the AR (and the HXR

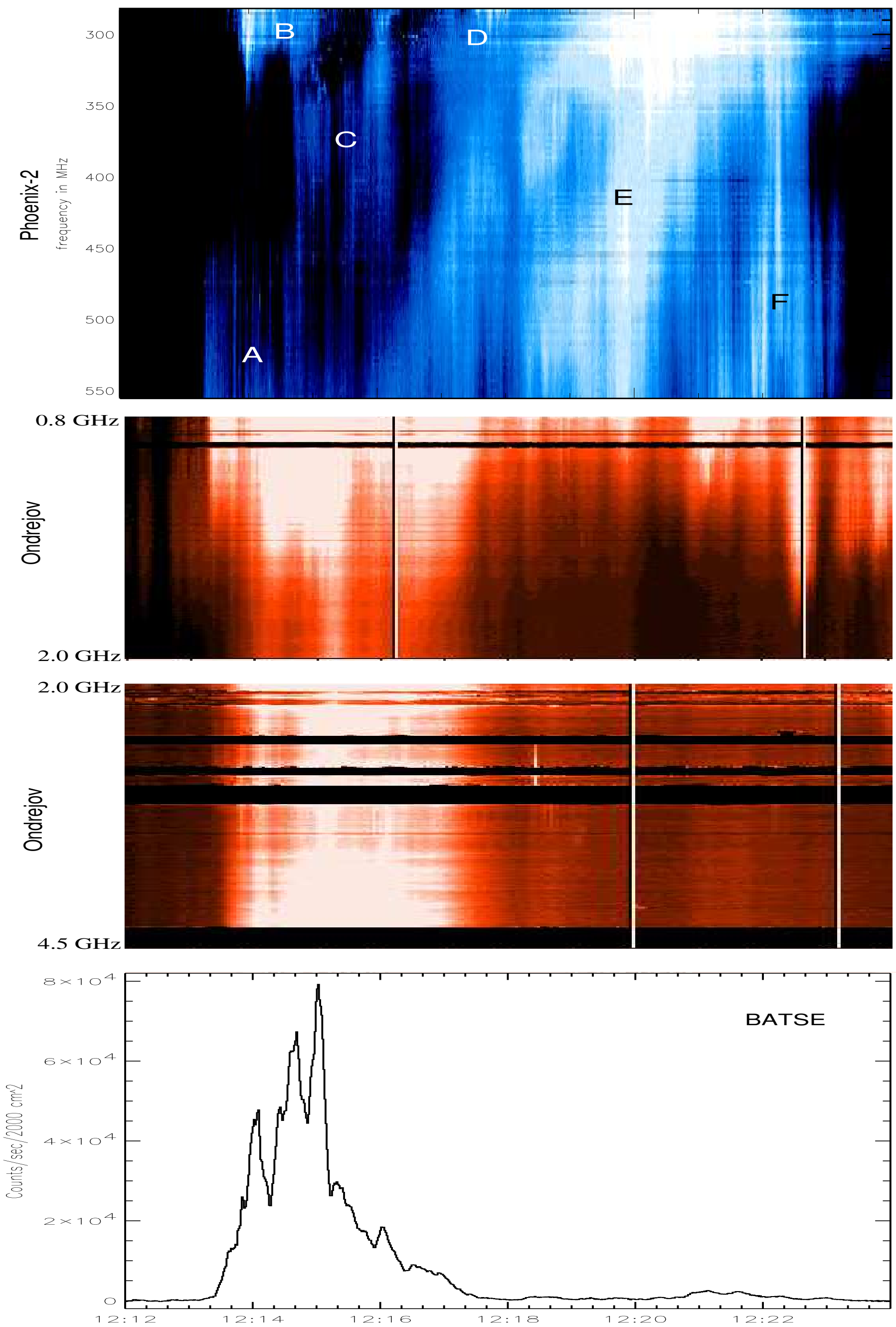


*Figure 4.* Time profiles for the 1999/09/08 event. The position of the emissions marked with letters is shown in Fig. 1 a-d. 'B' and 'D' are type III burts, whereas the others are DPS.

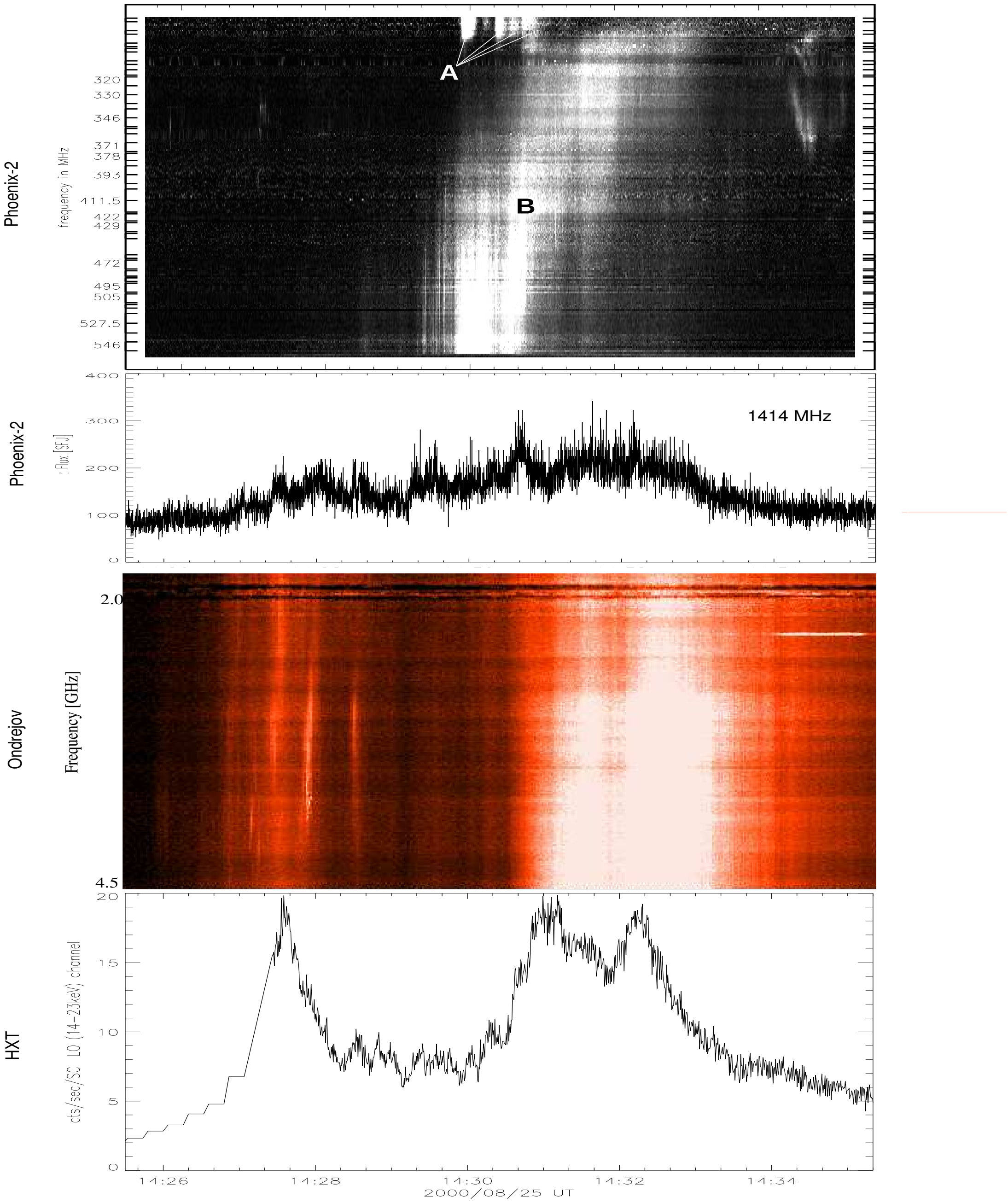


*Figure 5.* Time profiles for the 2000/08/25 event. The positions of the emissions 'A' and 'B' are shown in Fig. 2b. 'A' are metric type III bursts, 'B' is a DPS.

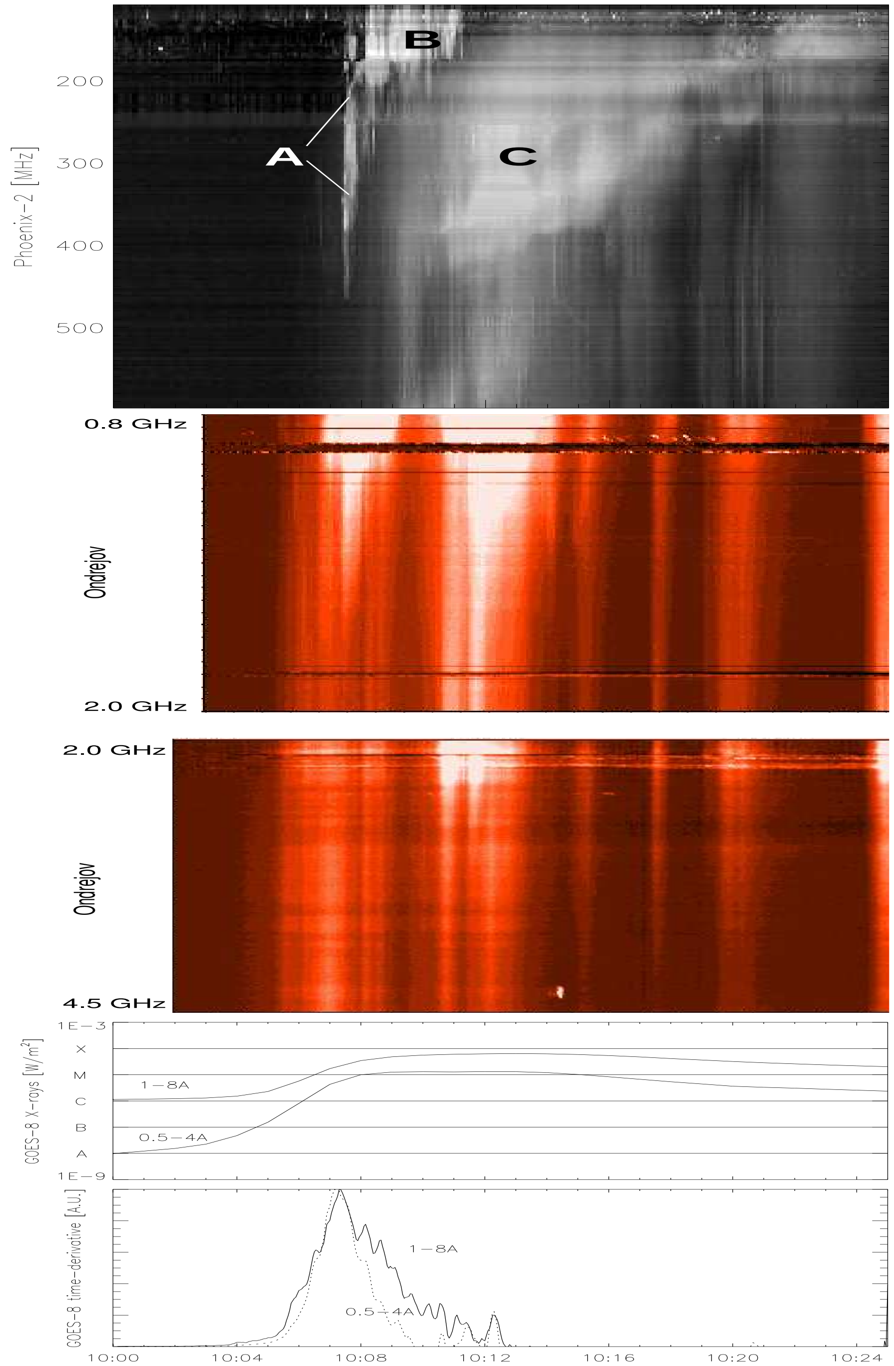


*Figure 6.* Time profiles for the 2001/06/15 event. 'A' is the "backbone" of the type II burst, 'B' is a group of metric type III bursts, and 'C' the DPS. Fig. 3 describes their location.

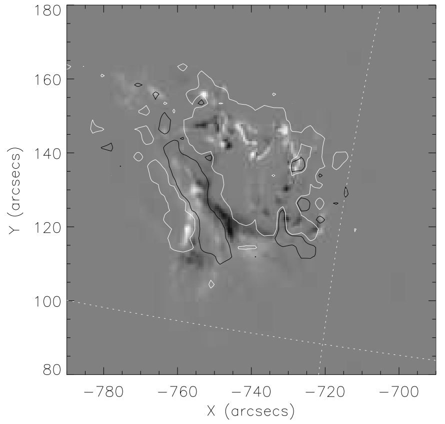


a. Difference TRACE and SXT (contour) image

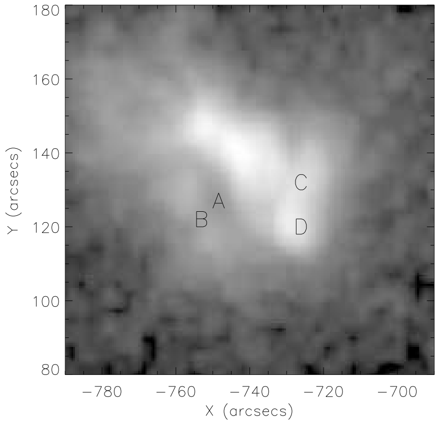


b. SXT image

*Figure 7.* (a) TRACE 1600Å difference image (12:13:54 minus 12:13:37 UT), where bright features represent an increase in brightness, and dark ones represent a decrease. Superposed are a set of SXT Al12 difference contours (12:13:59 minus 12:13:45 UT). The white contour shows the +1% level, the black contour the -1% level. (b) SXT Al12 image at 12:13:45 UT. The labels stand for regions where temperature and densities were determined, see text.

Table III. Temperature and densities of different positions in the AR for the 1999/09/08 event (Fig. 7). The real values are expected to lie within the nominal value given, multiplied or divided by the uncertainty factor.

| Pos. | Description | Te [MK] | Uncertainty factor | Density [$cm^{-3}$] | Uncertainty | Plasma frequency [GHz] |
|---|---|---|---|---|---|---|
| A | dim cavity between ejecta and AR | 13.8 | 2.3 | $2.1 * 10^9$ | 1.7 | 0.4115 |
| B | ejecta itself | 10.8 | 1.4 | $1.5 * 10^{10}$ | 1.1 | 1.1 |
| C | HXR footpoint | 9.3 | 1.1 | $8.4 * 10^{10}$ | 1.03 | 2.6 |
| D | location of the 327MHz emission | 8.7 | 1.1 | $7.9 * 10^{10}$ | 1.04 | 2.5 |

footpoints) during the HXR phase. They then slowly drift away from the AR, clearly in a loop-like pattern (see figures 1d, 3c and d, as well as their related movies). In the 2000/08/25 event, the DPS similarly drifts away from the AR, but also remains close to the main ejecta (the plasmoid - see Khan et al., 2002). This is particularly true for the 327 MHz channel. At the onset of DCIM emission, interestingly, the highest frequency NRH channels (410.5 and 432 MHz, and sometimes also 327 MHz) show sources very close to the AR: a few 10's of arcseconds for the 1999/09/08 and 2001/06/15 events, up to ~100" for the 200/08/25 event.

In other events where DPS were witnessed, such as the 2000/08/12 C3.2 flare and the 2000/09/14 C2.1 flare, the DPS also started at the same time as the HXR. In one case, the 2000/09/14 flare, it even started before, and was non-drifting, as are those events studied by Kliem et al. (2000).

A type II burst also occured in the 2001/06/15 event. It started before the DCIM, south of the AR (seemingly at a higher altitude), whereas the DCIM occured north of the AR.

The polarisation of the DCIM pulsations is variable from event to event (observed to be from 0 to about 50%), but remained approximately constant within an event. We also note for the 2001/06/15 event a DPS occurring ~0.5 hour after the HXR peak drifted to higher frequencies with a polarization opposite to that of the 'standard' DPS feature that occurred shortly after the HXR peak.

### 3.3. LASCO observations:

As a big CME was expelled an hour before the 1999/09/08 12:25 UT flare, which might explain why no CME was witnessed associated with this flare (the first CME was still going on and enhanced density such that the second event might have passed unseen). Starting on 2000/08/25 at 14:54, LASCO observations show a strong CME being expelled, from about the flare site, and with the same direction of travel as the ejecta. Starting on 2001/06/15 at 10:31, LASCO observations show a strong CME being expelled, from about the flare site, and with the same direction of travel as the ejecta.

## 4. Discussion

The fact that ejecta seem to be already on their way when hard x-rays are emitted would support the scenario of a driven magnetic reconnection, where magnetic energy is released rapidly because magnetic structures are pushed together. This is in contrast to the spontaneous reconnection model, where the local Lorentz force is responsible for the reconnection. On the other hand, in other similar events, no ejecta was witnessed. SXT only faintly saw the ejecta in the 1999/09/08 event, whereas TRACE's 1600 Å filter saw it very clearly. The ejecta (plasmoid) of the 2000/08/25 event was clearly seen by SXT, but only faintly by TRACE's 171 Å filter. From this, we speculate that ejecta may be often present, but too weak or not seen because at the wrong temperature with respect to the filters at our disposal.

Type IIIs occuring simultaneously with HXR result from accelerated electron beams, propagating along magnetic loops or open field lines that reach interplanetary space. They appear first at a far distance (80" in Fig. 1a) from the HXR source. The very weak sources at 410 and 432 MHz are not much further in, suggesting that the acceleration of the type III electrons may be at high altitude.

What causes the DCIM emission ? The individual pulsations could be due to electrons trapped at the edges of the ejecta. In a widely accepted scenario, electrons trapped in coronal magnetic loops develop a loss-cone distribution which is unstable and supports plasma emission at the fundamental or harmonic of the local upper-hybrid frequency (Kuijpers and Slottje, 1976).

This is the hypothesis that Khan et al. (2002) defend: the detected radio emission comes from trapped particles in the vicinity of a plasmoid, which would account for the fact that the radio sources moves with the plasmoid (or ejecta). It is the case of the 2000/08/25 event, but obviously not of the 1999/09/08 and 2001/06/15 events. In the 2000/08/25 event, the DCIM was clearly seen to follow the ejecta/plasmoid. In the 1999/09/08 and 2001/06/15 events, the DCIM was initially very close to the AR at HXR peak flux time, but then moved further away in a loop-like pattern (that was in the path of the ejecta in the 1999/09/08 event, but on the ejecta's path in the 2001/06/15 event). The discrepancy actually suggests two different situations, although their respective spectrograms are very much alike, and exhibit the same features.

In particular, what causes the pulses seen in all of the events studied in this paper ? NRH measurements show brightness temperatures above $10^{11}$ K, if one corrects for pulse time vs. integration time. This value might easily be orders of magnitudes higher, since our radio sources seem not to be resolved. This then precludes any non-coherent emission mechanism such as gyrosynchroton emission (Dulk, 1985). Additionally, a broader-band emission would have been expected from such a mechanism.

As seen in Table I, the individual pulses exhibit very high drift rates, more than 1000 MHz/s. These can generally not come from *broadband spikes* emitted from one localized source, as the group delay (e.g. Benz, 2002) would lead to negative-only drift rates, and we do observe positive drift rates. Another possibility is the *extended source* scenario (e.g., a magnetic loop with an oscillating diameter), where the source is modulated simultaneously at all frequencies. The drift rate is then given by the variable source distance from the observer (Aschwanden and Benz, 1986):

$$\frac{\partial \nu}{\partial t} = + \frac{\nu\, c\, \cos(\theta)}{2\, H_n \cos(\phi)}, \tag{1}$$

where $\theta$ is the angle between the source's main extension and the radial direction from the Sun, $\phi$ is the angle between the source's main extension and the observer's line of sight, $\nu$ is the center frequency, $c$ the speed of light, and $H_n$ is the density scale height. The drift rates for the 1999/09/08 event would easily fit an extended source with $\theta =$ 15.1 degrees and $\phi = 51.8$ degrees. This scenario seems plausible for both the plasmoid (2000/08/25 event) scenario, and for the majority of cases (such as the 1999/09/08 and 2001/06/15 events), where the DCIM seem to originate from a single, loop-like structures. We would expect from such a structure to produce predominently positive drift rates (which is the case), as high frequencies, being produced further down in the corona, reach us last (on the other hand, Aschwanden and Benz (1986) report also negative drift rates for such structures). We might expect to see another similar 'mirror' footpoint. The fact that this was not witnessed might be due to beaming or refraction effects.

Assuming alternatively that the emission originates from *electron beams* propagating in the corona, the drift rate (treated in a proper relativistic fashion) is given by:

$$\left(\frac{\partial \nu}{\partial t}\right)_{Rel} = - \frac{\nu\, c\beta \cos(\theta)}{2\, H_n \,(1 - \beta \cos(\phi))} \tag{2}$$

where $\beta$ is the beam velocity (in units of c). It was assumed that the speed of propagation of the radiation is constant throughout the corona, and equal to the speed of light in vacuum (this assumption must be taken, as the group velocity varies along the path of the radiation: from close to zero at $\omega \approx \omega_p$ to almost the speed of light at $\omega \approx 2\omega_p$).

According to Eq. (2), no drift rate observed and occuring in the hemisphere nearest us can be higher than $+\frac{c\nu}{2\,H_n}$, at least for beams propagating at less then $0.7c$. This means that $\frac{\dot{\nu}}{\nu}$ cannot be higher than +1.5, assuming a barometric 2 MK atmosphere. The ratio of $\frac{\dot{\nu}}{\nu} \geq +2.33$ observed in Table I would imply that the radio emission takes place in a region where the corona is cooler than 1.3 MK. This might be the case sometimes, but is probably not the rule, as we would need for a sizable portion of the corona to have a lower then expected temperature, wherever and whenever the DCIM emission occurs!

Another possibility are beams of electrons going through temporary inhomogeneities in the corona. Such inhomogeneities could have scale heights as small as a few tens of kilometers. Taking our drift rate of

$\frac{\dot{\nu}}{\nu} = 2.33 = +\frac{V_h}{H}$, and $H$ about 85 km, a value of $V_h \sim 200$ km/s is obtained, a typical ejecta or (slow) solar wind velocity.

Among the proposed emission mechanisms, the beam model in the case of an inhomogeneous corona seems a likely candidate, although the extended source scenario cannot be ruled out.

## 5. Conclusions

To summarize, here are the main points:

- major HXR flares are often associated with ejecta seen in SXR and/or EUV.

- ejecta seem to start before HXR or DCIM emission, suggesting a driven reconnection process.

- DCIM continua occuring nearly simultaneously with the first HXR peak are located close to the HXR source and may be a good indicator of the location of the main acceleration region.

- LASCO: a CME was observed 20 to 30 minutes after the flare in most cases.

- the main DCIM pulsations seem to be emitted by particles possibly trapped in the legs of magnetic loops carried outwards by the ejecta/plasmoid and are apparently not associated with the initial acceleration mechanism responsible for the HXR emission.

- in flares not in our selection, features like ejecta and DCIM pulsations are not always apparent, even during strong flares: possibly due to ejecta temperature and radio propagation in the corona.

- DCIM is apparently not gyromagnetic, nor from broadband emission spike in origin, but could be from extended sources or from type III burst-like emissions occuring in density inhomogeneities.

- metric type III bursts occur within $\sim$1-2 min after first peak in the HXR flux. Faint decimetric type III bursts were sometimes observed to occur a $\sim$1-4 minutes before the first HXR peak.

- DCIM observed at high frequencies are generally better related to the HXR timing and located closer to the HXR source. This observation opens the possibility that future observations of DCIM at even higher frequencies (1 - 3 GHz) may find them even nearer and thus closer to the main acceleration region.

## 6. Acknowledgements

We wish to acknowledge the team operating the Nançay Radioheliograph for providing their data through the on-line BASS-2000 database, and some discussions on the data, particularly with Alain Kerdraon and Nicole Vilmer, the SURF and YDAC on-line archives for the Yohkoh and TRACE data, and the Ondrejov Astronomical Institute for their high-frequency radio spectrograms. Special thanks to Hugh Hudson for his help on the Yohkoh software, and to Bob Bentley, for his on-line analysis guides. This research was made possible through the Swiss National Fond grant 20-67995.02 and ETH grant TH-W1/99-2.

## References

Aschwanden, M.J., Benz, A.O.: 1986, *Astron. Astrophys.* **158**, 102
Aschwanden, M.J., Benz, A.O.: 1988, *Astrophys. J.* **332**, 447
Aschwanden, M.J., Benz, A.O., Kane, S.R.: 1990, *Astron. Astrophys.* **229**, 206
Aschwanden, M.J., Schwartz, R.A., Dennis, B.R.: 1998, *Astrophys. J.* **502**, 468
Benz, A.O.: 1986, *Solar Phys.* **104**, 99
Benz, A.O., Csillaghy, A., Aschwanden, M.J.: 1996, *Astron. Astrophys.* **309**, 291
Benz, A.O., Saint-Hilaire, P., Vilmer, N.R.: 2002, *Astron. Astrophys.* **383**, 678
Benz, A.O., Plasma Astrophysics, 2nd ed.: 2002, Kluwer Academics Publishers, Dordrecht
Bruggmann, G., Benz, A.O., Magun, A., Stehling, W.:1990, *Astron. Astrophys.* **240**, 506
Dulk, G.A., Radio emission from the Sun and stars: 1985, *Ann. Rev. Astron. Astrophys.* **23**, 169
Fishman, G.J., *et al.*: 1989, Proc. GRO Science Workshop **2**, 39
Guedel, M., Benz, A.O.: 1990, *Astron. Astrophys. Suppl. Ser* **75**, 243
Guedel, M., Benz, A.O., Aschwanden, M.J.: 1991, *Astron. Astrophys.* **251**, 285
Handy, B., *et al.*: 1999, *Solar Phys.* **187(2)**, 229
Hori, K., 1999, in Solar Physics with Radio Observations, Proceedings of the Nobeyama Symposium, NRO Report No. 479, p. 267
Isliker, H., Benz, A.O.: 1994, *Astron. Astrophys. Suppl. Ser* **104**, 145
Jiricka, K., Karlick, M., Kepka, O., Tlamicha, A.: 1993, *Solar Phys.* **147**, 203
Karlicky, M., Farwik, F., Meszarosova, H.: 2002, *Astron. Astrophys.* **388**, 1016
Kerdraon, A., Delouis, J.-M.: 1996, in: Coronal Physics from Radio and Space Observations, Trottet G. (ed.), Springer Verlag, Berlin, 192
Khan, J.I., Vilmer, N.R., Saint-Hilaire, P., Benz, A.O.: 2002, *Astron. Astrophys.* **388**, 363
Kliem, B., Karlický, M., Benz, A.O.: 2000, *Astron. Astrophys.* **360**, 715
Kosugi, T., Makishima, K., et al.: 1991, *Solar Phys.* **136**, 17
Krucker, S., Aschwanden, M.J., Bastian, T.S., Benz, A.O.: 1995, *Astron. Astrophys.* **302**, 551
Kuijpers, J., Slottje, C.: 1976, *Solar. Phys.* **46**, 247
Messmer, P., Benz, A.O., Monstein, C.: 1999, *Solar Phys.* **187 (2)**, 335
Miller, J.A., *et al.*: 1997, *J. Geophys. Res.* **102/A7**, 14631

Miller, J.A.: 1998 CESRA Workshop on Coronal Explosive Events, held 9-13 June, 1998. Metsaehovi Publications on Radio Science, HUT-MET-27, 1998, p. 11. ISBN 951-22-4097-1, ISSN 1455-9587

Paesold, G., Benz, A.O., Klein, K.-L., Vilmer, N.: 2001, *Astron. Astrophys.* **371**, 333

Roberts, B., Mangeney, A.: 1982, *Mon. Not. R. Astr. Soc.* **198**, 7

Tsuneta S., et al.: 1991, *Astrophys. J.* **459**, 342